MULTIFRAGMENTATION OF LEAD NUCLEI AT 158 *A*GeV

A. Dąbrowska, M. Szarska, A. Trzupek, W. Wolter and B. Wosiek

The H. Niewodniczański Institute of Nuclear Physics
Kawiory 26a, 30-055 Kraków, Poland

(Received August 31, 2001)

Multifragment emission following Pb–Pb and Pb–Plastic collisions at 158 *A*GeV has been studied with a set of emulsion chambers of the EMU13 CERN experiment. It was found that the probability of nuclear multifragmentation increases with increasing mass of the target nucleus. For Pb–Pb collisions, multifragmentation events represent more than 30 % of the total charge changing cross section. On the other hand characteristics of multifragmentation are found to be independent of the mass of the target. A comparison is made with the results for Au multifragmentation after the collisions with emulsion nuclei at lower energies. The results suggest that above 10 *A*GeV the features of multifragmentation processes are energy independent.

PACS numbers: 25.75.+r, 29.40.Rg

1. Introduction

Multifragmentation is a complex nuclear reaction in which an excited nucleus disintegrates into several intermediate mass nuclear fragments. Over more than a decade, a number of experimental studies as well as theoretical works has been devoted to the investigation of this process. The expected association of the multifragmentation to the liquid-gas phase transition in nuclear matter [1] stimulated this activity. A recent status on multifragmentation can be found in [2]. Many of experimental results supported the hypothesis of the first order phase transition [3]. Despite this substantial body of evidence, there is still on going debate on the precise theoretical explanation of multifragmentation. Some experimental data are well explained by the statistical description of the process at and after the freeze-out [4]. Others suggest that intermediate mass fragments are dynamically produced [5].

Most of available experimental data on multifragmentation were obtained at low energies (below 1 AGeV). In this paper we extend these studies to the multifragmentation of lead projectiles at an energy of 158 AGeV. The analyzed data were obtained from the CERN EMU13 experiment in which emulsion chambers were exposed to the beam of ^{208}Pb ions accelerated in SPS. Emulsion chambers, composed of nuclear target foils and thin emulsion plates interleaved with spacers, allow for precise measurements of emission angles and charges of all projectile fragments emitted from Pb-Nucleus interactions. The results on fragment multiplicities, charge distributions and angular correlations are analyzed for multifragmentation of the Pb projectile after an interaction with heavy (Pb) and light (Plastic — $C_5H_4O_2$) targets. In addition, we also test the validity of Zipf's law, recently proposed as a signature of the nuclear liquid-gas phase transition. Data on Au-Emulsion interactions at lower energies are used to study the energy dependence of the nuclear multifragmentation.

The paper is organized as follows. In Section 2 a brief description of experimental details is given. In Section 3 the properties of the Pb(158 AGeV) multifragmentation are shown for the two collision systems: Pb–Pb and Pb–Plastic interactions. The comparison between the Pb multifragmentation at 158 AGeV and that of gold nuclei at 10.6 AGeV and below 1 AGeV is presented in Section 4. A summary of our results and conclusions are given in Section 5.

2. Experiment

Several lead-emulsion chambers were irradiated by Pb nuclei accelerated in SPS at CERN to an energy of 158 AGeV. The chambers were composed of three different modules. The target module consisted of several 100 μm thick lead foils interleaved by emulsion plates. The angular measurement module contained emulsion plates and spacers. Each emulsion plate in the target and angular measurement module consisted of a 200 μm thick acrylic base coated with emulsion layer on each side. Finally, at the downstream end of the chamber, the charge module is located. Details of emulsion chambers used in this experiment as well as irradiation conditions can be found elsewhere [6,7].

Scanning for Pb–Pb and Pb–Plastic (acrylic base of emulsion plates) interactions was done under the microscope in the target module of the chambers. Details of scanning for Pb interactions have been comprehensively described in [6]. Angular measurements of singly charged particles and multiply charged projectile fragments, emitted from the interaction vertex within a forward cone of $\theta \leq 10$ mrad, were done using a CCD camera mounted on a microscope and coupled to the computer. This automatic device assured measurements of track coordinates with the sub-micron pre-

cision. Charge measurements of multiply charged projectile fragments were done by δ-ray counts in thick emulsion pellicles placed in the bottom module specially designed for charge measurements. The accuracy of charge determination was of the order of 10 % for charges greater than about 30 and of the order of 1–2 charge units for lighter fragments.

3. Target dependence of the multifragmentation of Pb projectile

Multifragmentation process is characterized by break-up of a heavy nucleus into many relatively light fragments. Due to the complexity of multifragmentation process there is no commonly accepted definition of an event being representative for multifragmentation. In the following we used simultaneously two criteria in order to select multifragmentation events. The number, N_f, of fragments heavier than helium must be greater than two, and the charge Z_1 of the heaviest fragment must not exceed half the value of Z_b, where Z_b is the sum of all charges of multiply charged fragments. The latter requirement assures that there is no leading, *i.e.* distinctly heavier, fragment among all multifragmentation products [8].

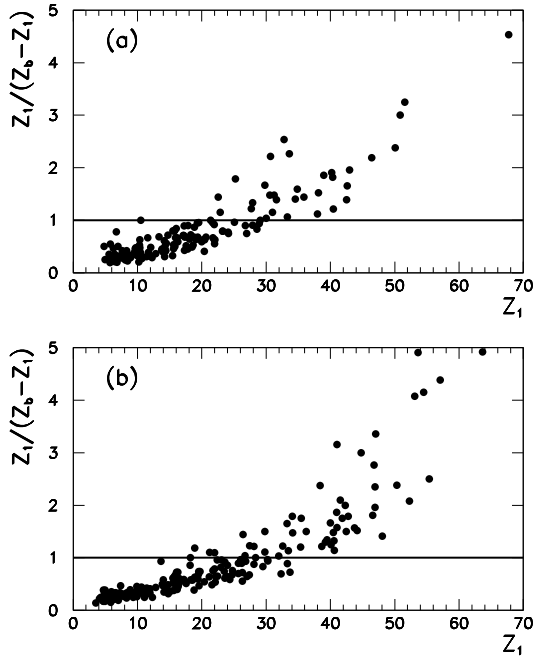

Fig. 1. Correlations between $Z_1/(Z_b - Z_1)$ and Z_1 for Pb–Pb (a) and Pb–Plastic (b) interactions with $N_f \geq 3$. Points below the horizontal lines represent our selection of multifragmentation events.

In Fig. 1 the correlation between the charge Z_1 of the heaviest fragment and the ratio $Z_1/(Z_b - Z_1)$ is shown for all Pb interactions with $N_f \geq 3$ on Pb (Fig. 1(a)) and Plastic (Fig. 1(b)) targets. Interactions without a leading fragment (multifragmentation events) are below the horizontal line. One can see that the definition of multifragmentation events used by us is equivalent to selecting events with more than two fragments heavier than helium and with the charge of the heaviest fragment (Z_1) not exceeding about 30. The ratio of multifragmentation events to all events with $N_f \geq 3$ equals $(76 \pm 7)\,\%$ and $(70 \pm 6)\,\%$ for Pb–Pb and Pb–Plastic interactions respectively. It should be emphasized that these samples of multifragmentation events are free of scanning biases, on the contrary to the inclusive samples of Pb–Pb and Pb–Plastic interactions where the scanning biases are significant [6], especially for peripheral collisions.

From the samples of measured Pb–Pb and Pb–Plastic collisions we have selected correspondingly 114 and 129 multifragmentation events. The experimentally measured cross section, σ_{mf}, for multifragmentation of Pb on Pb and Plastic target are correspondingly 2.4 ± 0.2 b and 0.40 ± 0.03 b. The ratios, $\sigma_{\mathrm{mf}}/\sigma_{\mathrm{tot}}$, of the multifragmentation cross sections to the calculated total nuclear charge changing cross section [9] are 0.35 ± 0.03 and 0.15 ± 0.01 for Pb and Plastic target, respectively. Thus, the multifragmentation processes are more frequent in collisions with heavy target nuclei as compared to the collisions with light targets. Processes of electromagnetic dissociation may be at least partially responsible for this difference [6].

In Table I mean values of some quantities measured in multifragmentation events for Pb–Pb and Pb–Plastic interactions are listed. One can see that average characteristics of multifragmentation events are independent of the mass of the target nucleus.

TABLE I

Mean numbers of helium, $\langle N_\alpha \rangle$, and heavier fragments, $\langle N_f \rangle$, the average charge $\langle Z \rangle$ of fragments heavier than helium, average charge $\langle Z_1 \rangle$ of the heaviest fragment and the average charge $\langle Z_b \rangle$ bound in multiply charged fragments are listed for the two samples of multifragmentation events.

	Pb–Pb	Pb–Plastic
$\langle N_\alpha \rangle$	5.8 ± 0.2	6.3 ± 0.2
$\langle N_f \rangle$	3.8 ± 0.1	3.9 ± 0.1
$\langle Z \rangle$	7.9 ± 0.3	7.7 ± 0.3
$\langle Z_1 \rangle$	14.1 ± 0.6	14.6 ± 0.7
$\langle Z_b \rangle$	41.9 ± 1.1	44.3 ± 1.2

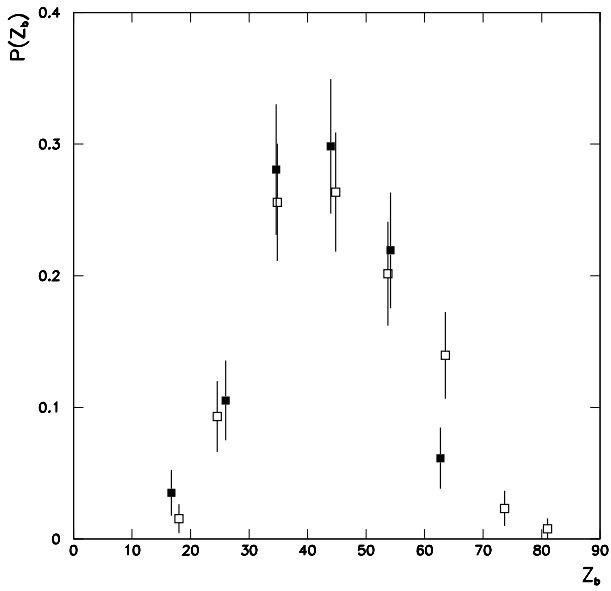

Fig. 2. Distributions of Z_b for multifragmentation Pb–Pb events (full squares) and Pb–Plastic events (open squares).

The distributions of the total charge Z_b bound in multiply charged fragments in multifragmentation events are depicted in Fig. 2. The distributions do not significantly differ from each other, although we observe that for the light target the Z_b distribution extends to more peripheral collisions (large Z_b) as compared to the lead target. Both distributions are peaked in the vicinity of half the charge of the projectile nucleus. These distributions, however, differ appreciably from the Z_b distribution measured for inclusive sample of Pb–Pb interactions (see [6]), which is practically constant over the entire range of Z_b values. Assuming, that Z_b is related to the energy transferred to the spectator remnant of the projectile, *i.e.* large energy transfer corresponds to the small value of Z_b, and vice versa, one can argue that the multifragmentation of Pb nucleus predominantly occurs in collisions with a moderate energy transfer.

3.1. Multiplicity distributions of helium and heavier fragments

Helium fragments are observed in different fragmentation processes. They are also present in multifragmentation events. In Fig. 3 we show the integral multiplicity distributions of helium fragments in multifragmentation of Pb projectile in collisions with Pb and Plastic targets. It can be seen that large multiplicities of helium fragments are more probable in Pb multifragmentation on lighter target than in Pb–Pb multifragmentation events.

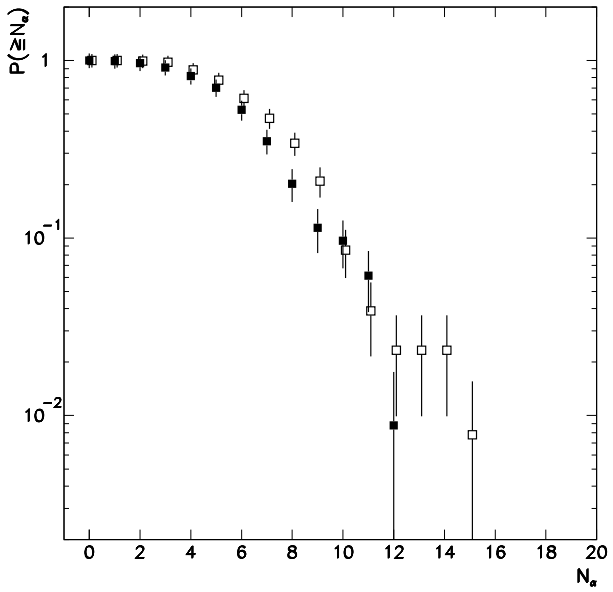

Fig. 3. Integral frequency distributions of the number of helium fragments. Symbol descriptions are the same as in Fig. 2.

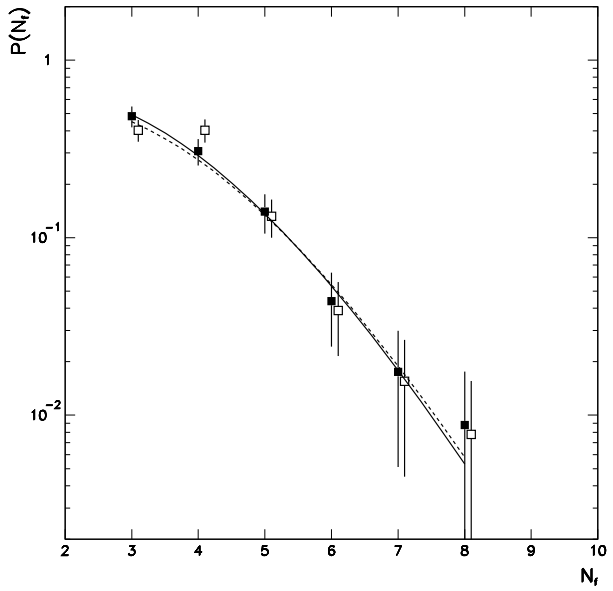

Fig. 4. Multiplicity distributions of N_f fragments. Lines show Poisson fits to Pb–Pb (solid line) and Pb–Plastic (dashed line) data. Symbols are the same as in previous figures.

In Fig. 4 the multiplicity distributions of fragments heavier than helium are shown. The distributions for Pb and Plastic targets coincide and they are well described by the Poisson distribution (χ^2/ndf is 0.14 and 1.60 for Pb and Plastic targets, respectively). It should be noted that the Poissonian distribution of fragments favors the statistical nature of multifragmentation process.

3.2. Charge distribution of fragments with Z≥ 3

In Fig. 5 we plot the charge distributions of fragments with Z $\geq$ 3 for Pb–Pb and Pb–Plastic interactions. The distributions are fitted by the exponential dependence (Fig. 5(a)), $P(Z) \sim \exp(-\mu Z)$ with the fitted value of $\mu = 0.19 \pm 0.01$ (χ^2/ndf = 1.6) for Pb–Pb and $\mu = 0.20 \pm 0.02$ (χ^2/ndf = 3.0) for Pb–Plastic multifragmentation events. Within the statistical errors the two distributions coincide.

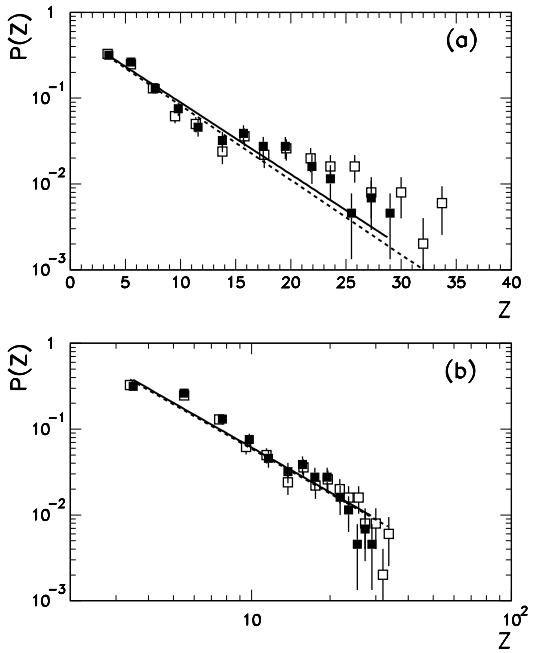

Fig. 5. Charge distributions of fragments with $Z \geq 3$. The lines are exponential (a), and power law (b) fits to the data.

It has been customary to fit the charge distributions of these fragments with the power law, $P(Z) \sim Z^{-\tau}$ (see *e.g.* [10]). This follows from the anticipated power law dependence of charge distribution of fragments with Z $\geq$ 3, with $\tau \approx 2.3$, in the case of a liquid-gas phase transition in the excited

nuclear matter [11]. On the other hand a recent analysis [12] of the critical exponents, performed within a framework of statistical multifragmentation model, predicts smaller values for the τ exponent. It is argued [12] that τ values falling into a narrow range $1.799 < \tau < 1.846$ should indicate that the critical point of the liquid-gas phase transition has been reached. Our data, when fitted by the power law (see Fig. 5(b)), give low values for the τ coefficients, namely 1.73 ± 0.08 and 1.72 ± 0.07, respectively, for Pb–Pb and Pb–Plastic data samples. However, the quality of the fits is poor ($\chi^2/\mathrm{ndf} = 3.0$ for Pb–Pb and $\chi^2/\mathrm{ndf} = 2.6$ for Pb–Plastic).

To summarize, our data do not allow distinguishing between exponential and power law description of fragment charge distributions. Neither of these functional forms can well describe the data.

3.3. Azimuthal correlations between fragments with $Z \geq 3$

The azimuthal angle (φ) correlations are sensitive to the accuracy of the beam axis determination. In this study of multifragmentation process we are mainly focused on the properties of intermediate mass fragments (N_f). Therefore, for every event we define the beam axis *i.e.* the center of the plane (x, y) perpendicular to the beam direction as charge weighted center of the measured coordinates of all N_f fragments. The azimuthal angles of fragments are then recalculated with respect to this beam axis.

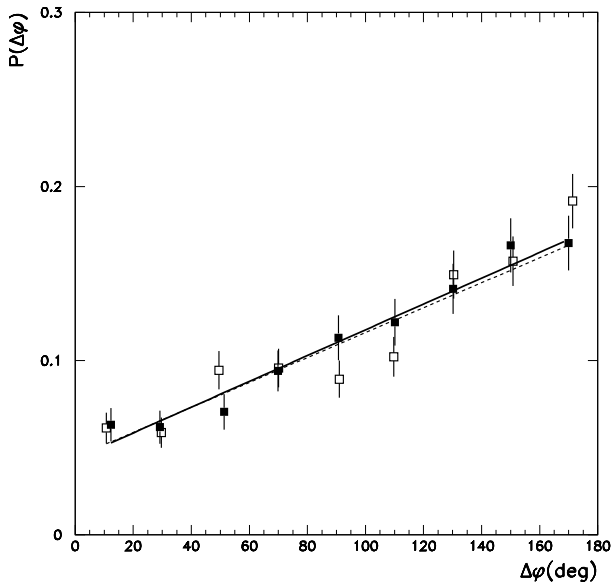

Fig. 6. Distributions of relative azimuthal angles between N_f fragments emitted in multifragmentation Pb–Pb (full squares, solid line) and Pb–Plastic (open squares, dashed line) events. Lines show linear fits to the data points.

In Fig. 6, the distributions of the relative azimuthal angles, $\Delta\varphi$, between fragments heavier than helium in multifragmentation of Pb on Pb and Plastic targets are shown. Both distributions are similar and differ from the isotropic ones. The yield of large values of $\Delta\varphi$ is greater than the yield of small ones. The azimuthal asymmetry coefficient, A, defined as:

$$A = \frac{\int\limits_{\pi/2}^{\pi} N(\Delta\varphi)d\Delta\varphi - \int\limits_{0}^{\pi/2} N(\Delta\varphi)d\Delta\varphi}{\int\limits_{0}^{\pi} N(\Delta\varphi)d\Delta\varphi}, \tag{1}$$

equals 0.315 ± 0.015 for Pb–Pb and 0.305 ± 0.014 for Pb–Plastic interactions. This shows that fragments are more often back-to-back emitted which may indicate that they are produced from a single source. Coulomb repulsion for high-Z fragments contributes also to this effect.

3.4. Application of Zipf's law to nuclear multifragmentation

Zipf's law [13] has been known as a statistical phenomenon, related to the critical behavior, which appears in the field of linguistics and also in other fields of sciences. Recently, the Zipf law has been applied [14, 15] to the charge distribution of fragments produced in nuclear fragmentation processes. It states that the relation between the fragment sizes and their ranks is described by $\langle Z_n \rangle = c/n$, where c is a constant and $\langle Z_n \rangle$ is the average charge of fragments of rank n in the charge list arranged in the order of decreasing size. To test the validity of the Zipf law, we average the charges for each rank and examine the goodness of the relation between $\langle Z_n \rangle$ and n with the fit $\langle Z_n \rangle \sim n^{-\lambda}$. When λ is close to one, the Zipf law is satisfied. In the theoretical calculations [14] it was shown that at the critical point of a liquid-gas phase transition the Zipf law should be valid ($\lambda \approx 1$). In Fig. 7 we present the average charge of fragments with $Z \geq 3$ as a function of its rank. The fitted values of λ are 0.88 ± 0.03 ($\chi^2/\mathrm{ndf} = 2.6$) and 0.96 ± 0.04 ($\chi^2/\mathrm{ndf} = 2.1$) for Pb and Plastic targets, respectively. These values are not very different from $\lambda \approx 1$. We can conclude that our multifragmentation data are approximately consistent with the Zipf law.

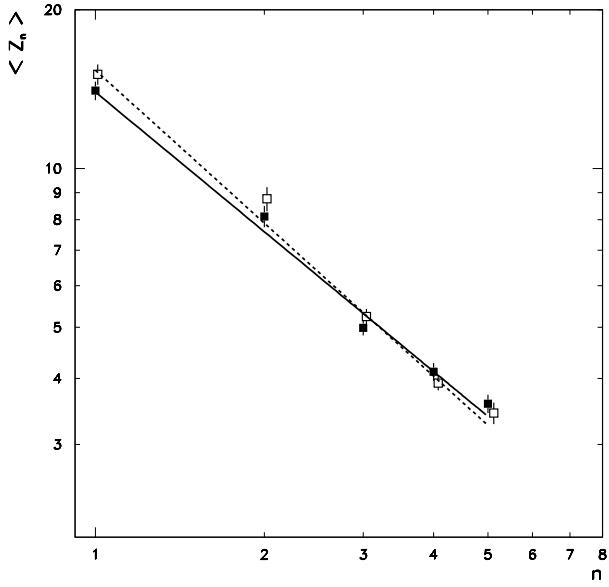

Fig. 7. Mean values of the charge of the fragment as a function of its rank. Lines show power law fits to the data points. Symbol and line descriptions are the same as used before.

4. Energy dependence of multifragmentation of heavy nuclear projectiles

In the previous section we have shown that the analyzed characteristics of the multifragmentation of the Pb projectile are essentially independent of the mass of the target nucleus. We disregard small differences observed in Z_b distributions and in the multiplicity distributions of helium fragments. This allows us to investigate the energy dependence of parameters characterizing multifragmentation process by comparing Pb data at 158 AGeV with the multifragmentation of Au projectiles at 10.6 AGeV [8,10] and below 1 AGeV [10, 16] interacting with the emulsion target. The average primary energy for the latter sample is 0.64 AGeV. For this comparison the Pb–Pb and Pb–Plastic data samples were pooled together, and for each data set the same criteria for selecting multifragmentation events were applied (as described in Section 3.).

In Table II we present the mean values of the same parameters as in Table I but for three different projectile energies. It can be seen that, while the properties of the two high energy samples do not differ, low energy data show significantly larger multiplicities of helium fragments and also larger Z, Z_1 and Z_b average values.

TABLE II

The same parameters as in Table I for the three different energies of the projectile nuclei.

	Pb(158 AGeV)	Au(10.6 AGeV)	Au(0.64 AGeV)
$\langle N_\alpha \rangle$	6.1 ± 0.2	6.5 ± 0.2	8.0 ± 0.3
$\langle N_f \rangle$	3.9 ± 0.1	3.9 ± 0.1	4.2 ± 0.1
$\langle Z \rangle$	8.1 ± 0.2	7.6 ± 0.2	8.6 ± 0.3
$\langle Z_1 \rangle$	14.6 ± 0.4	13.7 ± 0.4	16.4 ± 0.8
$\langle Z_b \rangle$	43.7 ± 0.8	42.3 ± 0.7	52.0 ± 1.2

The distributions of Z_b/Z_p, where Z_p is the charge of the primary nucleus, for the three different primary energies are depicted in Fig. 8. For 10.6 AGeV and 158 AGeV the distributions cover the same range of Z_b/Z_p values, with the mean values around half the charge of the primary. However, for 0.64 AGeV the distribution is shifted towards larger values of Z_b/Z_p. This means that, at this low energy, there is more multifragmentation events with less energy transfer to the spectator remnant than at higher energies. In another words multifragmentation at low primary energies occurs in more peripheral collisions than at high energies.

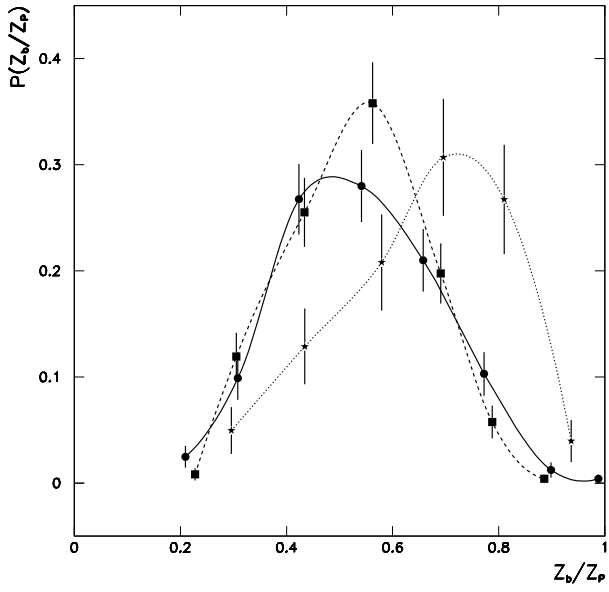

Fig. 8. Distributions of Z_b/Z_p for multifragmentation of Pb projectile at 158 AGeV (circles), Au projectile at 10.6 AGeV (squares) and Au projectile at $\langle E \rangle = 0.64$ AGeV (stars). Curves are added to guide the eye.

It was observed [10] that the mean multiplicity of helium fragments from Au projectiles in multifragmentation events depends on primary energy being shifted to lower values at 10.6 AGeV in comparison with 0.64 AGeV data sample. Note that in [10] slightly different criteria for selecting multifragmentation events were applied. In order to check whether the observed energy dependence holds for still higher energies, we compared the multiplicity distributions of helium fragments in multifragmentation events for the three data sets, selected with the same criteria used in this paper. This comparison is presented in Fig. 9. One can see that the scaling of multiplicity distribution of helium fragments from the multifragmentation of heavy nuclei (Au, Pb) holds for energies above 10.6 AGeV.

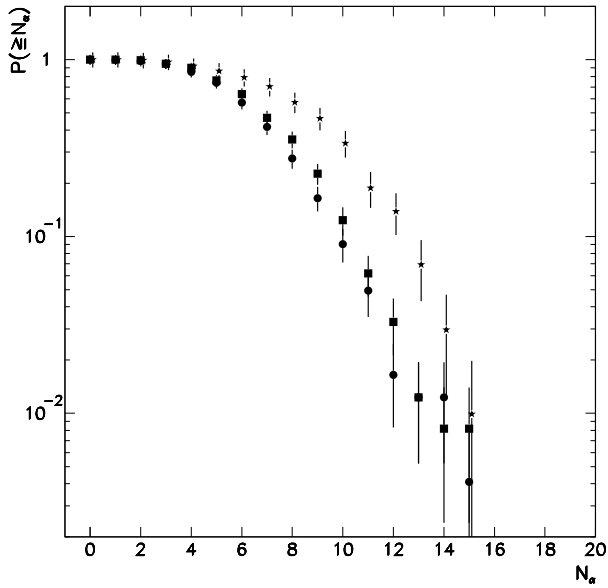

Fig. 9. Integral frequency distributions of helium fragments. See Fig. 8 for symbol explanations.

The Poissonian multiplicity distribution of fragments with Z $\geq$ 3 was also observed for multifragmentation of Au projectiles in interactions with nuclear emulsion [10]. In Fig. 10 we compare our present data at 158 AGeV with those for Au multifragmentation at 10.6 AGeV and 0.64 AGeV . The higher energy data are well described by the Poisson distribution (χ^2/ndf = 0.76 and 1.41 for 10.6 AGeV and 158 AGeV, respectively) whereas the quality of the Poissonian fit (χ^2/ndf = 2.94) is worse for the lowest energy data.

Concluding, we can say that the multiplicity distributions of helium and heavier fragments from the multifragmentation processes of heavy nuclei (Au, Pb) are the same for 10.6 AGeV and 158 AGeV primary energy, but

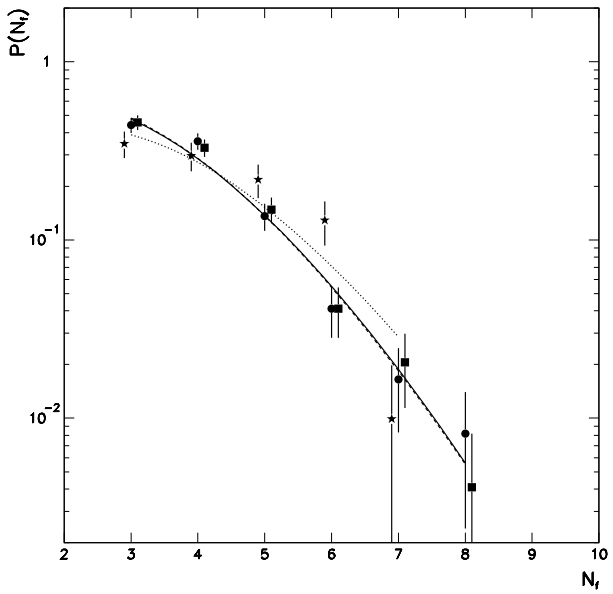

Fig. 10. Poisson fits to the multiplicity distributions of N_f fragments for multifragmentation of Pb at 158 AGeV (circles, solid line), Au at 10.6 AGeV (squares, dashed line), and Au at 0.64 AGeV (stars, dotted line).

differ from those observed below 1 AGeV. The yield of large helium fragment multiplicities at 0.64 AGeV primary energy is greater than that at higher energies. The same tendency we observe for fragments with Z $\geq$ 3.

The charge distribution of fragments heavier than helium for the three data samples are the same, within statistical errors, and their description by either exponential or power law fit is equally poor.

In Fig. 11 we present the results of the analysis of the Zipf law for the charged fragments heavier than helium emitted in multifragmentation processes of Au or Pb projectile at different primary energies. The values of λ exponents from fits $\langle Z_n \rangle \sim n^{-\lambda}$ are: 0.92 ± 0.03 ($\chi^2/\mathrm{ndf} = 4.0$), 0.90 ± 0.02 ($\chi^2/\mathrm{ndf} = 0.4$) and 0.96 ± 0.04 ($\chi^2/\mathrm{ndf} = 0.7$) for primary energies of 158, 10.6 and 0.64 AGeV, respectively. Within the statistical errors the values of the λ coefficient are the same in the studied energy interval ($<$ 1–158) AGeV, and do not differ significantly from unity.

We also checked the energy dependence of the azimuthal correlations between fragments heavier than helium using the Au–Em data at 10.6 AGeV and Pb–(Pb + Plastic) data at 158 AGeV. The results are presented in Fig. 12. The distributions are identical and deviate from uniformity.

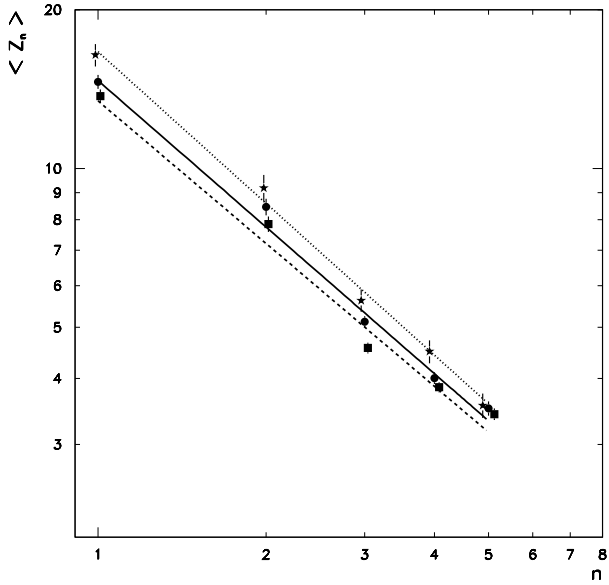

Fig. 11. Power law fits to the dependence of the mean charge of the fragment on its rank. Symbol and line descriptions are the same as in Fig. 10.

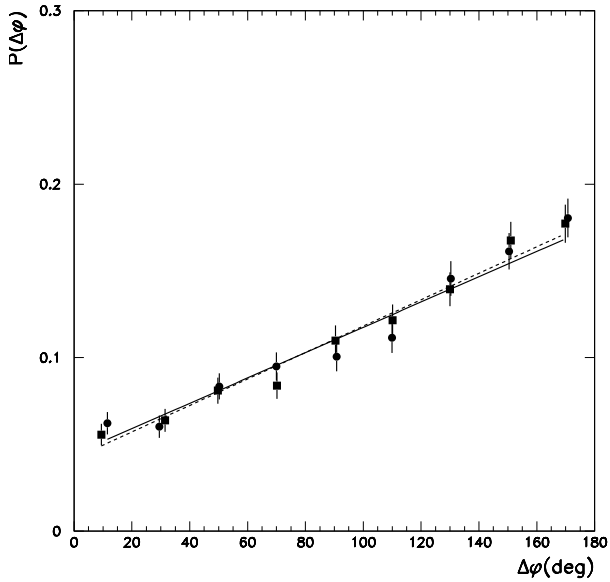

Fig. 12. Distributions of relative azimuthal angles between N_f fragments for Pb multifragmentation at 158 AGeV (circles, solid line) and Au multifragmentation at 10.6 AGeV (squares, dashed line). Lines show linear fits to the data points.

5. Summary and conclusions

We investigated the multifragmentation process of Pb projectile nuclei at 158 AGeV in collisions with Pb and Plastic targets. We found that the multifragmentation of Pb nucleus is more frequent in collisions with heavy target nuclei. On the other hand, the quantities describing the multifragmentation process, like the multiplicity of fragments with $Z \geq 3$ and their charge characteristics, do not depend on the mass of the target. Small differences are only observed in the yields of helium fragments, which are larger in collisions with Plastic target than in Pb–Pb multifragmentation events. The Z_b distribution measured for the Plastic target exhibits a tail extending to large Z_b values which is not seen for Pb–Pb events.

The distribution of the charge bound in multiply charged fragments indicates that at 158 AGeV the multifragmentation process frequently occurs in collisions with a moderate energy transfer to the spectator remnant. The multiplicity distributions of fragments are well described by the Poisson distribution, pointing to the statistical character of multifragmentation process. The distributions of the relative azimuthal angles between the fragments are asymmetric. The fact that fragments are more frequently emitted back-to-back in the plane perpendicular to the beam axis may indicate that they originate from a common source.

We also tested the Zipf law, which, according to the theoretical calculations, should be valid when applied to fragments in multifragmentation events. Our data are roughly consistent with the Zipf law. This may be interpreted as an evidence for the existence of the critical temperature associated with a liquid-gas phase transition.

Energy dependence of the multifragmentation process was also studied by analyzing fragmentation of gold projectiles at 10.6 and below 1 AGeV after collisions with the emulsion target and our combined data sample of Pb–(Pb + Plastic) interactions at 158 AGeV. In general the process of nuclear multifragmentation at 158 AGeV does not differ from that at 10.6 AGeV. However, at much lower energies the differences are observed. Below 1 AGeV, the process predominately takes place in more peripheral collisions than at higher energies and the yields of helium and heavier fragments are larger. Charge distributions as well as the relation between size of the fragments and their rank do not exhibit significant energy dependence over the full investigated energy range.

This work was partially supported by the Polish State Committee for Scientific Research (KBN) Grant 2P03B05417.

REFERENCES

[1] L.G. Moretto *et al.*, *Phys. Rep.* **287**, 249 (1997).

[2] Proc. of Int. Workshop XXVII on Gross Properties of Nuclei and Nuclear Excitation, Hirschegg, Austria, Jan. 17-23, 1999, Edited by H. Feldmeier, J. Knoll, W. Norenberg, J. Wambach, GSI, Darmstadt 1999.

[3] B. Borderie `nucl-ex/0102016`; J.B. Elliott *et al.*, `nucl-ex/0104013`.

[4] R.P. Scharenberg *et al.*, `nucl-ex/0107015`.

[5] J. Toke *et al.*, *Phys. Rev.* **C56**, R1683 (1997).

[6] M.L. Cherry *et al.*, *Acta Phys. Pol.* **B29**, 2155 (1998).

[7] P. Deines-Jones *et al.*, *Phys. Rev.* C**53**, 3044 (1996); *Phys. Rev.* **C62**, 014903 (2000).

[8] M.L. Cherry *et al.*, *Phys. Rev.* **C52**, 2652 (1995).

[9] B.S. Nilsen *et al.*, *Phys. Rev.* **C52**, 3277 (1995); L.Y. Geer *et al.*, *Phys. Rev.* **C52**, 334 (1995).

[10] A. Dąbrowska *et al.*, *Acta Phys. Pol.* **B31**, 725 (2000).

[11] A.D. Panagiotou *et al.*, *Phys. Rev. Lett.* **52**,496 (1984).

[12] P.T. Reuter, K.A. Bigaev, `nucl-th/0104090`.

[13] G.K. Zipf, *Human Behaviour and the Principle of Least Effort*, Addisso-Wesley Press, Cambridge MA 1949.

[14] Y.G. Ma, *Eur. Phys. J.* **A6**, 367 (1999).

[15] Y.G. Ma, *Phys. Rev. Lett.* **83**, 3617 (1999).

[16] C.J. Waddington, P.S. Freier, *Phys. Rev.* **C31**, 388 (1985).